A FRAMEWORK FOR INTEGRATED COMPONENT AND SYSTEM ANALYSES OF INSTABILITIES

Vineet Ahuja, James Erwin and Srinivasan Arunajatesan
Combustion Research and Flow Technology, Inc.
6210 Keller's Church Road
Pipersville, PA 18947

Lou Cattafesta and Fei Liu
University of Florida
231 MAE-A P. O. Box 116250
Gainesville, FL 32611

ABSTRACT

Instabilities associated with fluid handling and operation in liquid rocket propulsion systems and test facilities usually manifest themselves as structural vibrations or some form of structural damage. While the source of the instability is directly related to the performance of a component such as a turbopump, valve or a flow control element, the associated pressure fluctuations as they propagate through the system have the potential to amplify and resonate with natural modes of the structural elements and components of the system. In this paper, the authors have developed an innovative multi-level approach that involves analysis at the component and systems level. The primary source of the unsteadiness is modeled with a high-fidelity hybrid RANS/LES based CFD methodology that has been previously used to study instabilities in feed systems. This high fidelity approach is used to quantify the instability and understand the physics associated with the instability. System response to the driving instability is determined through a transfer matrix approach wherein the incoming and outgoing pressure and velocity fluctuations are related through a transfer (or transmission) matrix. The coefficients of the transfer matrix for each component (i.e. valve, pipe, orifice etc.) are individually derived from the flow physics associated with the component. A demonstration case representing a test loop/test facility comprised of a network of elements is constructed with the transfer matrix approach and the amplification of modes analyzed as the instability propagates through the test loop.

INTRODUCTION

Rocket engine and component testing facilities are usually comprised of an assembly of elements such as cavitating venturis, orifices, turbopumps, turning ducts and control valves that are networked together in a configuration that meets design goals and testing requirements. The complexity in the flowpath of such configurations, however, has the potential of introducing flow induced instabilities due to vortex shedding, cavitation, turbulence and large scale flow separation. Such flow phenomena are usually accompanied by pressure fluctuations that can interact with test system components as well as test articles such as pumps and combustors. Alternately, the pressure fluctuations can also arise from the transient stages of testing such as during engine start-up, shutdown or during sudden changes in thrust levels. The pressure fluctuations, whether due to flow instability or transient testing, may excite certain structural modes and can lead to system wide resonance, thereby compromising the safety of the test stands and leading to premature shutdown of tests. Such deleterious structural vibrations coupled with large scale pressure fluctuations have been known to lead to system malfunction as has been seen in the case of the Delta 4 system. A good example of this coupling is represented by a commonly known phenomenon called the "POGO" instability where a closed loop interaction develops between longitudinal structural modes of vibration and the instability dynamics of the propulsion system (feed lines and tanks). The instability propagates into the pumps where fluctuating inlet pressures result in cavitation leading to oscillating thrust, which in turn amplifies the longitudinal structural modes that set the instability in motion in the first place.

From an analysis perspective, the instability mechanisms seen in testing facilities can be classified into three distinct classes: (a) acoustic/hydrodynamic/fluid dynamic instabilities [1] that are predominantly attributed to fundamental flow physical mechanisms such as vortex shedding, turbulence, etc. largely associated with complex structural configurations such as valve housing, plug shapes, manifolds and bends in the piping system. (b) flow transients associated with valve timing and valve scheduling [2]. Such transients can play an important role especially during startup\shutdown and valve response can be critical for safe and reliable operation. The water hammer instability, being a prime example, of rapid shutdown of a valve leading to large amplitude pressure fluctuations in the system. (c) multi-phase instabilities such as cavitation related instability mechanisms [3] that become especially important with cryogenic working fluids due to reduced liquid to vapor density ratios and strong evaporative cooling effects resulting in local temperature fluctuations that can couple with the primary cavitation instability.

It has become commonplace to use specialized CFD based numerical tools to identify the above-mentioned instability modes and the dominant frequencies associated with them. For example, high fidelity computational analyses have been performed for a series of structurally complex valve systems such as the pressure regulator valve, split-body valve and globe valves. Such simulations have been usually carried out with an advanced hybrid RANS-LES turbulence framework [4] that has permitted accurate representation of a rich spectrum of spatial and temporal scales very efficiently. Moreover, a novel valve motion computational technique coupled with a grid movement algorithm has been used to simulate transient motion of valves during operation. This has permitted analyses of valve scheduling procedures and prediction of transients during valve operations. Coupled fluid-structure simulations of valve systems have also been undertaken to predict structural response to the governing flow instability [5]. In such simulations the effects of the valve packing/dampers have also been included and consequently its feedback and the fluid response have been captured.

For application to flows with multi-phase instabilities the CFD framework was enhanced with sub-models for unsteady cavitation and real fluid thermodynamic property routines [6]. These developments have facilitated the simulation of two-phase regimes in cryogenic fluids where phase change and temperature fluctuations are strongly coupled to pressure and flow variations. Analysis of cavitation instabilities such as traveling cloud cavitation have been performed for control elements in test loops such as venturis and orifices as well as rotating cavitation for high pressure inducers/turbopumps.

While the high fidelity CFD simulations discussed above have been successful at identifying the physical mechanisms responsible for the fluid instabilities and the fundamental modes associated with these instabilities, uncertainties persist on the coupling of the instability modes with the functioning of other elements in the test loop, their response to the instabilities, and consequently the resulting structural excitation and vibrations in the piping. In spite of the large strides made by computational hardware technology, it is still extremely expensive to analyze the entire test loop utilizing high-fidelity LES simulations that resolve most of the scales of unsteadiness. System modeling tools on the other hand, are either limited in scope such as studies reported on transient pipe flows that neglect components such as orifices, valves and the instabilities associated with them, or oversimplify the physical mechanisms inherent in these components. There are two approaches used to model system components that can be used in conjunction with high-fidelity CFD. The first approach uses a Lumped Element Model (LEM) which is based on the representation of the governing physical parameters (flow coefficient, structural compliance) of the components by equivalent electronic analogues (resistance, capacitance) in an electrical circuit [7]. The second approach assigns a transfer matrix (TM) to each component that relates inflow perturbations with outflow responses. The TM for a particular component can be derived mathematically from physical theory governing the working of a component, experimental or testing data, or computational analysis. TM techniques have been applied successfully to acoustic problems [8], and cavitation instability problems with turbopumps [9] and are a viable option for simulating the effects of instabilities in ducts, diffusers and flow control elements in rocket propulsion testing facilities. In the next few sections we discuss the TM approach and derive representative forms of the transfer matrix for common components seen in test facilities such as ducts, bends and orifices. We examine a Kelvin Helmholtz instability using high fidelity CFD and subsequently derive an equivalent TM from the CFD computations. Lastly, we discuss the propagation of an instability in a scaled down test loop which comprises of a duct, an orifice, a bend and a diffuser using the TM approach.

Approved for public release; distribution is unlimited.

Copyright © 2010 by the authors. Published by JANNAF with permission. All rights reserved.

RELEASED - Printed documents may be obsolete; validate prior to use.

TRANSFER MATRIX APPROACH

A transfer matrix (TM), also known as a transmission matrix, T-matrix, or ABCD matrix, is traditionally employed in electrical and mechanical vibration theory [10]. In both fields, the analysis of complicated systems has been greatly simplified by the use of this method. Complex circuits or structures can be simply regarded as a "two port network" with input and output ports, as shown in Figure 1. Matrix algebra can then be applied for analysis of such networks by linking the dynamic behavior between inputs and outputs through the coefficients of the matrix. The interconnection of parallel, series-parallel, and parallel-series network combinations can thus be handled by simple linear addition or multiplication of the transfer matrix. Since 1930, the transfer matrix method has also enjoyed considerable use in acoustic problems [11]. In the following sub-sections, we will develop the transfer matrices for the wave propagation through a uniform or variable-area duct with or without incompressible or compressible flow, an orifice, and a 90-degree bend, which comprises the test loop as shown in Figure 2.

Figure 1. A Two-Port Network.
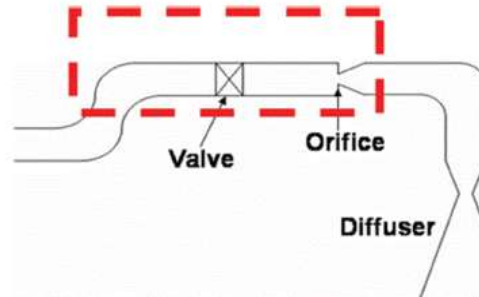
Figure 2. Illustration of a Test Stand which Consists of Ducts, an Orifice, and a 90° Bend.

TRANSFER MATRIX FOR A DUCT ELEMENT

The transfer matrix for a straight duct was derived for a wave propagating through the duct with and without a mean flow in a viscous medium that could either consist of an incompressible or compressible fluid. The pressure perturbation in the pipe is assumed to be smaller than the product of the density and square of the characteristic speed of sound, thereby permitting large pressure fluctuations, an important requirement for liquid rocket engine systems and test facilities. Furthermore, the transfer matrix accounts for viscous/thermal losses as well as the absorption of low frequency sound waves in the boundary layer of the pipe system. The detailed derivations and the theory are discussed in detail in [12]. The derived transfer matrix representation of the straight duct in its general form is given as

$$
\begin{bmatrix} p' \\ u' \end{bmatrix}_{x=l} = e^{jM_0 k_c l} \begin{bmatrix} \cos\ k_c l & -j\rho_0 c_0 \eta \sin\ k_c l \\ -\dfrac{j}{\rho_0 c_0 \eta}\sin\ k_c l & \cos\ k_c l \end{bmatrix} \begin{bmatrix} p' \\ u' \end{bmatrix}_{x=0}
\tag{1}
$$

where $k_c = \left[k_0 - j\ \alpha + \zeta M_0\ \right]\Big/ 1 - M_0^2$ where α and ζ represent the effects of viscous/thermal losses, k_0 is the incident wave number, l is the length of the duct and M0 is the characteristic Mach Number. The effects of viscous friction, heat conduction and acoustic attenuation in the boundary layer included in the derivation here are extensively dealt in Refs. [13], [14]. Under its various approximations, the general form of transfer matrix can be reduced as follows:

No viscothermal loss

$$
\eta = 1, k_c = \frac{k_0}{1 - M_0^2}
\tag{2}
$$

3

$$\begin{bmatrix} p' \\ u' \end{bmatrix}_{x=l} = e^{jM_0 k_c l} \begin{bmatrix} \cos\ k_c l & -j\rho_0 c_0 \sin\ k_c l \\ -\dfrac{j}{\rho_0 c_0}\sin\ k_c l & \cos\ k_c l \end{bmatrix} \begin{bmatrix} p' \\ u' \end{bmatrix}_{x=0}$$

(3)

No mean flow with negligible visco-thermal loss

$$\eta = 1, k_c = k_0 \tag{4}$$

$$\begin{bmatrix} p' \\ u' \end{bmatrix}_{x=l} = \begin{bmatrix} \cos\ k_0 l & -j\rho_0 c_0 \sin\ k_0 l \\ -\dfrac{j}{\rho_0 c_0}\sin\ k_0 l & \cos\ k_0 l \end{bmatrix} \begin{bmatrix} p' \\ u' \end{bmatrix}_{x=0}$$

(5)

COMPARING ANALYTICAL AND EXPERIMENTAL RESULTS

In this section, the comparison between the transfer matrix derivation for the 1-D wave propagation within a duct with mean flow and the experimental data is demonstrated. The experimental results are presented in [15]. For demonstration, a rectangular duct, as shown in Figure 3, is considered. The length of the duct is $l = 0.28\ m$ and the width and height are 0.12 m and 0.05 m respectively. The duct is driven by a speaker upstream and details for the experimental setup and acoustic measurement are shown in [15]. The mean flow velocities are set in the experiment to be M_0 = 0, 0.1, 0.2, and 0.3. The comparison is made for the case of hard-walls filling the openings for liner, as shown in Figure 3. The comparison results for a variety of Mach Numbers at an excitation frequency of 1500 Hz are shown in Figure 4. The results indicate that the TM predictions agree very well with the experimental data.

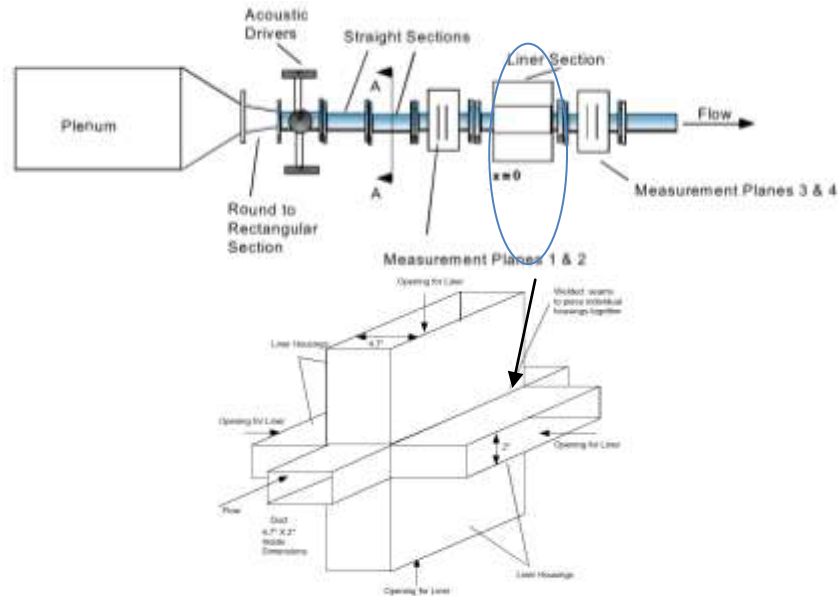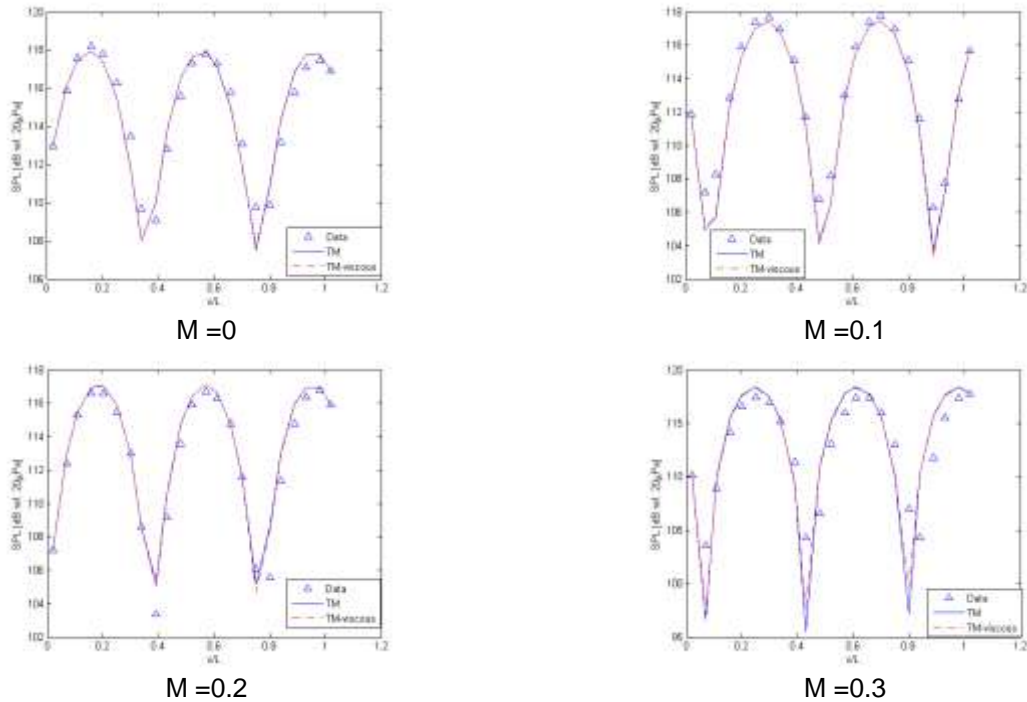**Figure 3. Illustration of the Experimental Facility and the Rectangular Duct as Defined in Ref. [15].**

4

M =0

M =0.1

M =0.2

M =0.3

Figure 4. The Acoustic Pressure at Sampling Points along the Central X-axis in a Rectangular Duct for various Mach numbers and f = 1500 Hz. Experimental data is compared against analytical TM formulations.

TRANSFER MATRIX FOR A VARIABLE AREA DUCT ELEMENT SUCH AS DIFFUSERS AND NOZZLES

The transfer matrix for a variable area duct/diffuser/nozzle is an extension of the one derived for the straight duct. However there are difficulties associated with the variation of the mean flow variables ρ_0, p_0, U_0 with area change. In such a case, the problem of finding a transfer matrix becomes complex because the acoustic differential equations (i.e., $\partial p'/\partial x$ and $\partial u'/\partial x$) have variable coefficients. Two approaches can be considered in extending the transfer matrix for the variable area duct. In the first approach [16], the variable area duct was defined as an accumulation of segmented straight ducts each with a slightly different area (see Figure 5(a)). In the second approach also discussed in Ref. [16], the profile of the variable area duct/nozzle/diffuser section was defined mathematically such as with an exponential function and each section (See Figure 5(b)) was assumed to be comprised of constant coefficients of acoustic differential equations (i.e., $\partial p'/\partial x$ and $\partial u'/\partial x$). The segment transfer matrices are then computed, and these matrices are multiplied sequentially to obtain the overall transfer matrix.
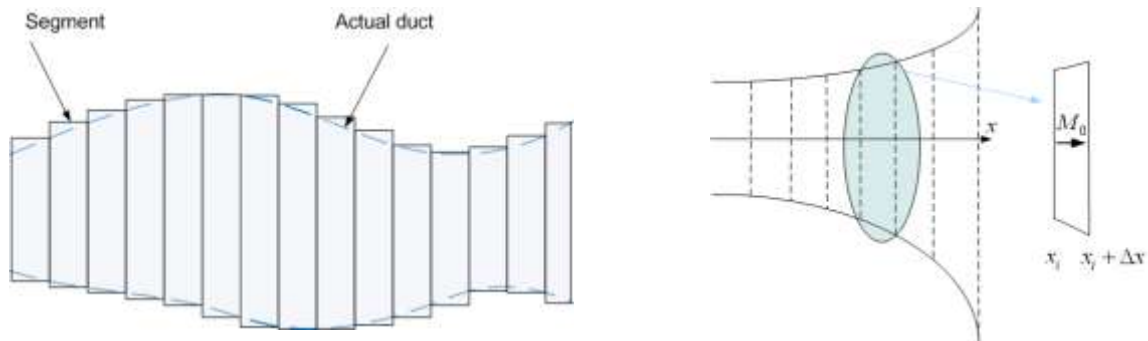
(a) Compilation of Constant Area Segments   (b) Variable Area for each Segment

Figure 5. Segmentation Strategies for Variable Area Duct.

5

Approved for public release; distribution is unlimited.

RELEASED - Printed documents may be obsolete; validate prior to use.

The first step is to derive the transfer matrix for each section with area change. This can be written as:

$$\underbrace{\begin{bmatrix} \partial p'/\partial x \\ \partial u'/\partial x \end{bmatrix}}_{\partial Y/\partial x} = \underbrace{\begin{bmatrix} B_{11} & B_{12} \\ B_{21} & B_{22} \end{bmatrix}}_{B} \underbrace{\begin{bmatrix} p' \\ u' \end{bmatrix}}_{Y}, \tag{6}$$

where all entries of the matrix B are as follows

$$B_{11} = \frac{M_0}{1-M_0^2} \, jk_0 \, - \frac{M_0^2}{1-M_0^2} \frac{\partial [\ln A]}{\partial x}, \tag{7}$$

$$B_{12} = -\frac{\rho_0 c_0}{1-M_0^2} \, jk_0 \, + \frac{2\rho_0 c_0 M_0}{1-M_0^2{}^2} \frac{\partial [\ln A]}{\partial x}, \tag{8}$$

$$B_{21} = -\frac{1}{1-M_0^2} \frac{1}{\rho_0 c_0} \, jk_0 \,, \tag{9}$$

and

$$B_{22} = \frac{M_0}{1-M_0^2} \, jk_0 \, - \frac{1+M_0^2}{1-M_0^2{}^2} \frac{\partial [\ln A]}{\partial x}. \tag{10}$$

The next step is to divide the duct into a number of segments. The size of the segment is selected so that the Mach number can be assumed constant in each segment and the cross-sectional area profile can be locally approximated as by an exponential variation as an example, in other words

$$M_0 = \text{const.}, \tag{11}$$

and

$$A = A_0 e^{mx}. \tag{12}$$

Hence, the gradient of the logarithmical variation of area is

$$\frac{\partial [\ln A]}{\partial x} = m. \tag{13}$$

Consequently, all entries of the matrix B are independent of x in each segment. The solution of Eqn. (6), i.e., $\partial Y/\partial x = BY$, is given by

$$Y\, x_i + \Delta x \, = e^{B\Delta x} Y\, x_i \,, \tag{14}$$

where Δx is the length of the i th segment. The value of $e^{B\Delta x}$ can be evaluated as

$$e^{B\Delta x} = I + B\Delta x + \frac{B\Delta x^2}{2!} + \frac{B\Delta x^3}{3!} + \dots, \tag{15}$$

So, the transfer matrix of the each segment is given be

$$T_i = \begin{bmatrix} T_{11} & T_{12} \\ T_{21} & T_{22} \end{bmatrix} = e^{B\Delta x}\Big|_{x_i} = \sum_{n=0}^{\infty} \frac{B\Delta x_i^{\,n}}{n!}, \tag{16}$$

The overall transfer matrix of wave propagation in a variable area duct is thus found from

6

$$T = \prod_i T_i.$$ (17)

For the sake of completeness, the derived matrix formulation was verified for the degenerate case of a straight duct and simple case for the special case of a conical pipe.

TRANSFER MATRIX FOR AN ORIFICE

A transfer matrix was also derived for an orifice-pipe system. The derivation assumed the mean flow to be uniform in the upstream duct, transition into a jet through the vena contracta, followed by a turbulent mixing region immediately downstream of the orifice, with flow recovery further downstream. The effect of a propagating perturbation is derived by applying the continuity and momentum equations in the turbulent mixing region downstream of the orifice, and defining the velocity and pressure variables as a combination of fluctuating and average quantities [17]. Subsequent linearization of the equations results in the coefficients of the transfer matrix.
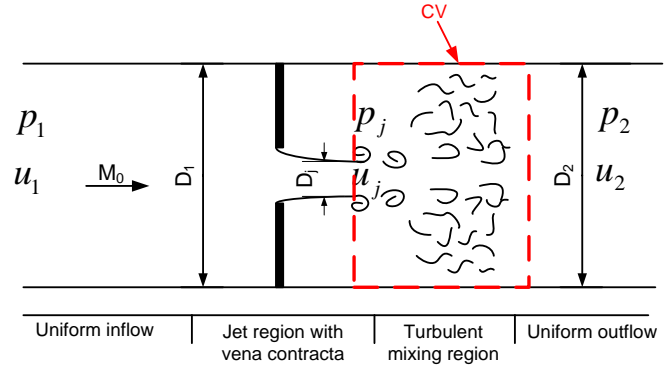
Figure 6. Schematic of a Quasi-Steady Flow Through an Orifice within a Duct.

The transfer matrix for the orifice can be written as

$$\begin{bmatrix} p_2' \\ u_2' \end{bmatrix} = \begin{bmatrix} 1 & -\rho_0 c_0 M_0 \beta \\ 0 & 1 \end{bmatrix} \begin{bmatrix} p_1' \\ u_1' \end{bmatrix},$$ (18)

where the coefficient, $\beta = S_p/S_j - 1^2$, represents the combination of the effect of the geometry and the vena contracta. It should be noted that the transfer matrix derived here does not account for the Kelvin Helmholtz instability initiated at the lip of the orifice. Extension of the TM to include the instability will be carried out in the future.

TRANSFER MATRIX FOR AN TURNING DUCT

Using a similar procedure as the orifice pipe system, a transfer matrix has also been derived for a disturbance/fluctuation passing through a sharp bend or a turning duct at low Strouhal Numbers [16]. The approach assumes that the flow separates behind the bend and the separated flow region acts as a blockage creating a natural vena contracta. The flow through the bend accelerates due to the reduced area formed by the vena contracta leading to a turbulent mixing region before the flow settles at the exit. Given the similarity to the flow dynamics of the orifice-duct system an analogous matrix was derived for sharp bends (radius of curvature to pipe diameter ratio (r/D) of less than 2) and turning ducts. The main distinction between the two matrices lies in the definition of the vena contracta. In the case of the orifice, the vena contracta is geometrically/structurally defined, whereas in the turning duct it is a function of flow characteristics such as Reynolds number as well as the curvature of the bend. The wall friction in the turbulent region is negligible

Hence, the transmission matrix for the wave propagating through the bend is given by

$$\begin{bmatrix} p_2' \\ u_2' \end{bmatrix} = \begin{bmatrix} 1 & -\rho_0 c_0 M_0 \beta \\ 0 & 1 \end{bmatrix} \begin{bmatrix} p_1' \\ u_1' \end{bmatrix}$$ (19)

Note that when the Mach number of the mean flow is larger than 0.3, the sharp bend is better described by a compressible quasi-steady flow theory [18]. The coefficient β depends on the extent of

7

the separation region (width), which in turn depends on the geometry of the bend and the characteristic Reynolds Number of the flow.

In the case of the smooth bend ($r \geq 2D$), as shown in Figure 8, it is not necessary to assume a free jet formation with a *vena contracta* at the bends. Thus, it may model the smooth bend as straight duct [18], as discussed in the previous section on the transfer matrix for straight ducts.
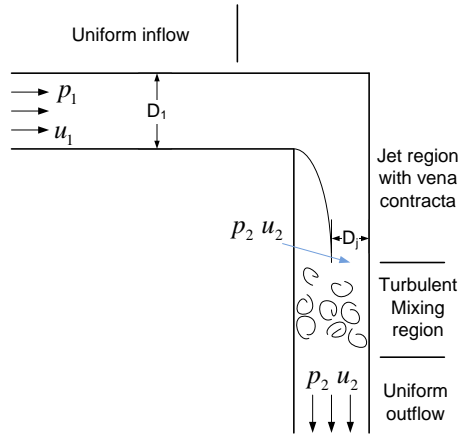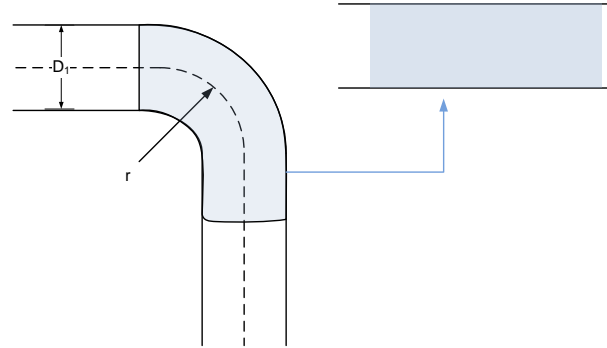

| Figure 7. Schematic of a quasi-steady flow through a bend within a duct. | Figure 8. Schematic of a quasi-steady flow through a smooth (r>D) bend within a duct. |

UNSTEADY CFD ANALYSES OF THE ORIFICE WITH HYBRID RANS/LES APPROACH

An orifice is routinely used in rocket engine test facilities to step down the pressure in a finite length of pipe and for flow control purposes. In this section, we discuss unsteady hybrid RANS-LES simulations of a pump discharge orifice in a stand-alone mode i.e. the orifice will not be coupled to any other flow components. The primary aim of this simulation is to characterize the instability that sets up in the orifice, understand the physics governing the unsteadiness and identify the unsteady modes related to the operation of the orifice.

Three-dimensional simulations were carried out of a pipe with a 4-inch diameter and an orifice with a vena contracta of 2.08 inches. The orifice is not a sharp edge slot type orifice but rather has a rounded shape to guide the flow smoothly to the vena contracta. This pipe-orifice configuration has been used for testing at NASA SSC with liquid oxygen as the operating fluid. The upstream pipe is long enough to ensure that the flow is well-developed before it encounters the orifice. The flow in the pipe has a mean velocity of 27.64 m/s, a temperature of 91.67 K and a characteristic Reynolds Number of approximately 4.2 million based on the pipe diameter. The time averaged solutions of pressure and velocity on the vertical plane are shown in Figure 9. The velocity distribution shows the flow accelerating through the orifice with a well defined jet extending to about a pipe diameter downstream of the orifice. Further downstream, the jet diffuses out to fill the pipe in the radial direction. The pressure distribution shows the pressure drop precipitously in the vena contracta and then recover about one diameter downstream of the orifice. While the drop in pressure on average is about 400 psi downstream of the orifice, a small pocket of very low pressure is formed in the vena contracta which may be susceptible to cavitation.


8
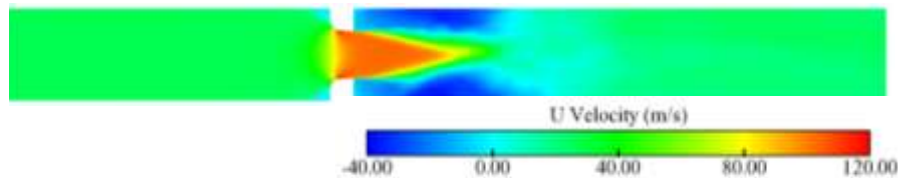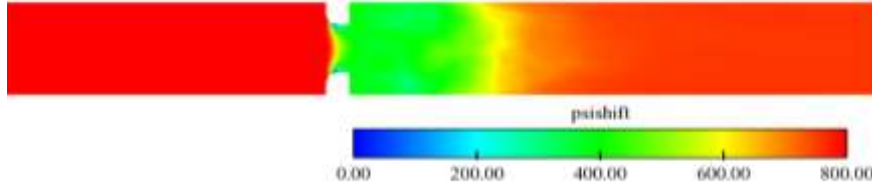
Figure 9. Time averaged solution of velocity and pressure distribution on the symmetry plane.
A series of snapshots of instantaneous velocity distribution is shown in

Figure 10 which indicates the formation of the primary jet as the flow accelerates to negotiate the orifice. This jet is representative of a high Reynolds Number flow due to the low viscosity of liquid oxygen. The snapshots of velocity distribution show the periodic generation of vortices from the lip of the orifice, the migration of the vortex structures into the downstream pipe section and subsequent dissipation of these structures further downstream in the pipe section. As a consequence of the production and dissipation of the vortex structures, and the dynamic interaction of the resultant jet with the wall, the length of the jet core is seen to periodically oscillate. The snapshots of pressure distribution are seen in Figure 11 which show spatially periodic patterns of low pressure (Figure 12) associated with the vorticity production at the lip of the orifice. The resulting Kelvin Helmholtz type instability in the pipe/orifice system leads to the unsteady shedding and the periodic formation of pockets of low pressure. Pressure traces from numerical probes located downstream of the orifice (after the jet expands radially in the pipe) show two important modes that are excited: (i) a high frequency mode of 180 Hz that corresponds to the Kelvin Helmholtz instability and (ii) a lower frequency mode of 45 Hz with an overtone at 90 Hz. The lower frequency mode is an axial mode that corresponds to the interaction of the jet with the pipe wall. This process is illustrated in the sequence of plots in Figure 13 where first we see the jet expanding radially in the pipe downstream of the orifice. Since the jet expands in the confined space of the pipe, the jet impinges on the pipe wall, and travels upstream toward the orifice creating a feedback loop, as the reverse flow interacts with the primary jet leading to a sub-harmonic of the primary Kelvin Helmholtz instability. The lower frequency mode also manifests itself as an axial instability causing the jet core to fluctuate in length.
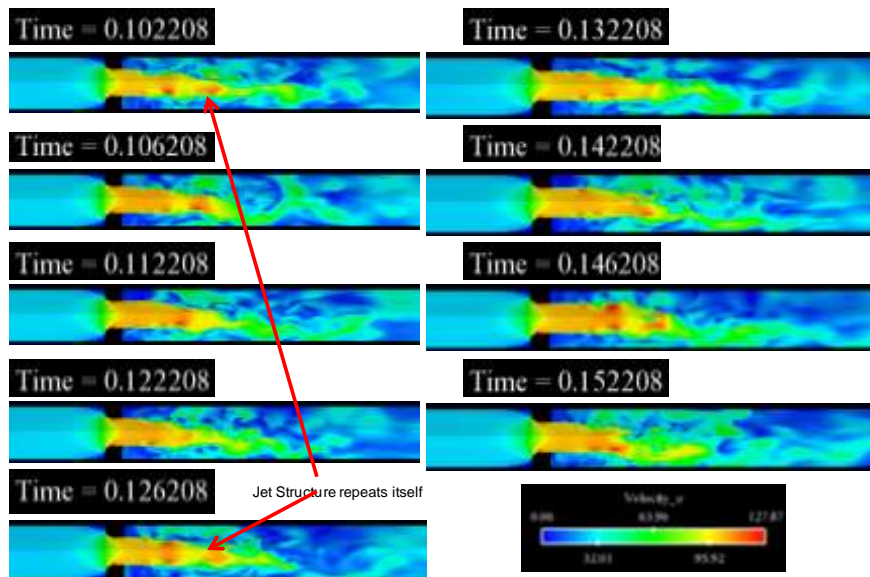
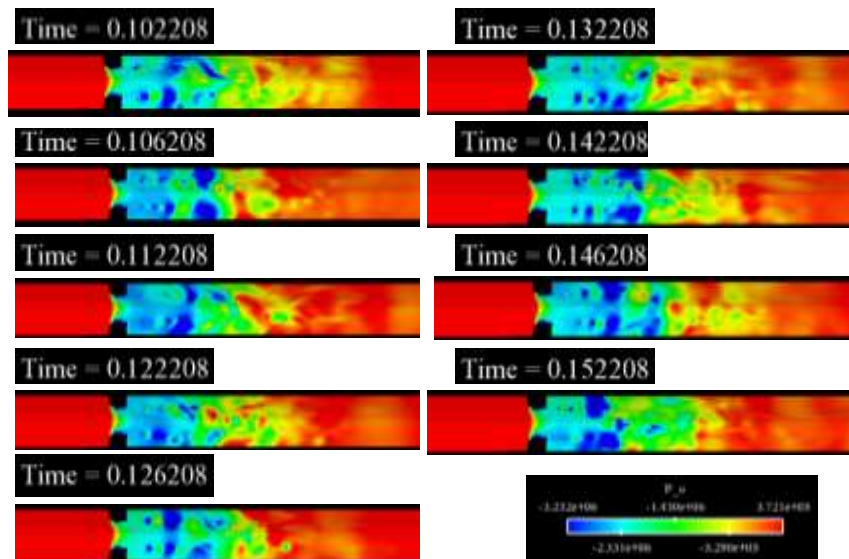**Figure 10. Snapshots of Instantaneous Axial Velocity Distribution.**

9

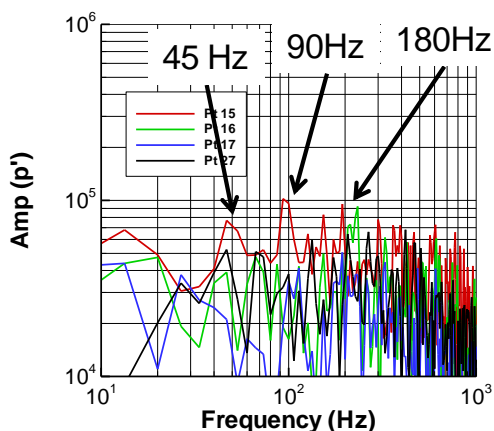**Figure 11. Instantaneous Snapshots of Pressure Distribution on the Vertical Plane.**

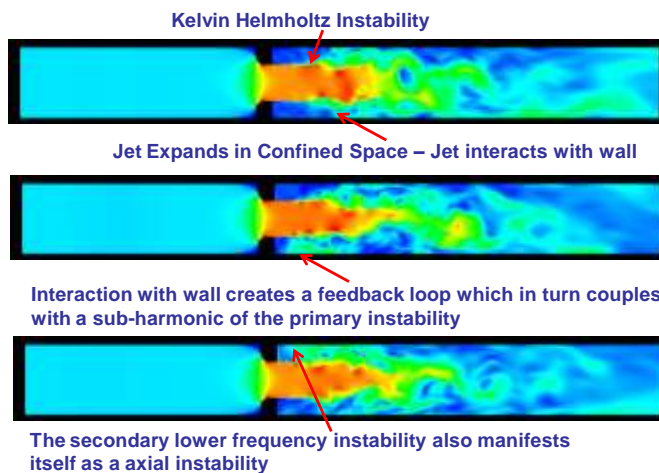**Figure 12. Pressure Spectra Showing Dominant Modes.**

Figure 13. Snapshots of Axial Velocity Distribution Showing the Evolution of the Instability Modes in the Computational Domain.

COMPUTATION OF TRANSFER MATRIX FROM CFD SIMULATIONS

Here we discuss the procedure used to compute the transfer matrix of a particular component directly from the CFD simulations. In the case of the orifice simulations, the history of pressure and velocity fluctuation was recorded by numerical probes at a series of points upstream and downstream of the orifice. For the purpose of demonstration we consider the fluctuation history at a point one-half inch upstream of the orifice and nine inches downstream of the orifice (See Figure 14). It is important to note here that (i) the downstream point is in the turbulent mixing region after the flow has re-attached to the wall and (ii) the fluctuations that are used in the derivation of the transfer matrix should be averaged across the cross-section plane rather than use isolated points as has been done in this demonstration case. The pressure and velocity spectra are shown in Figure 15 for both the points on the upstream and downstream sides.

RELEASED - Printed documents may be obsolete; validate prior to use.

Figure 14. Orifice Domain Showing location of the Upstream Probe(31) at x=-0.5 and Downstream Probe(15) located at x=9.
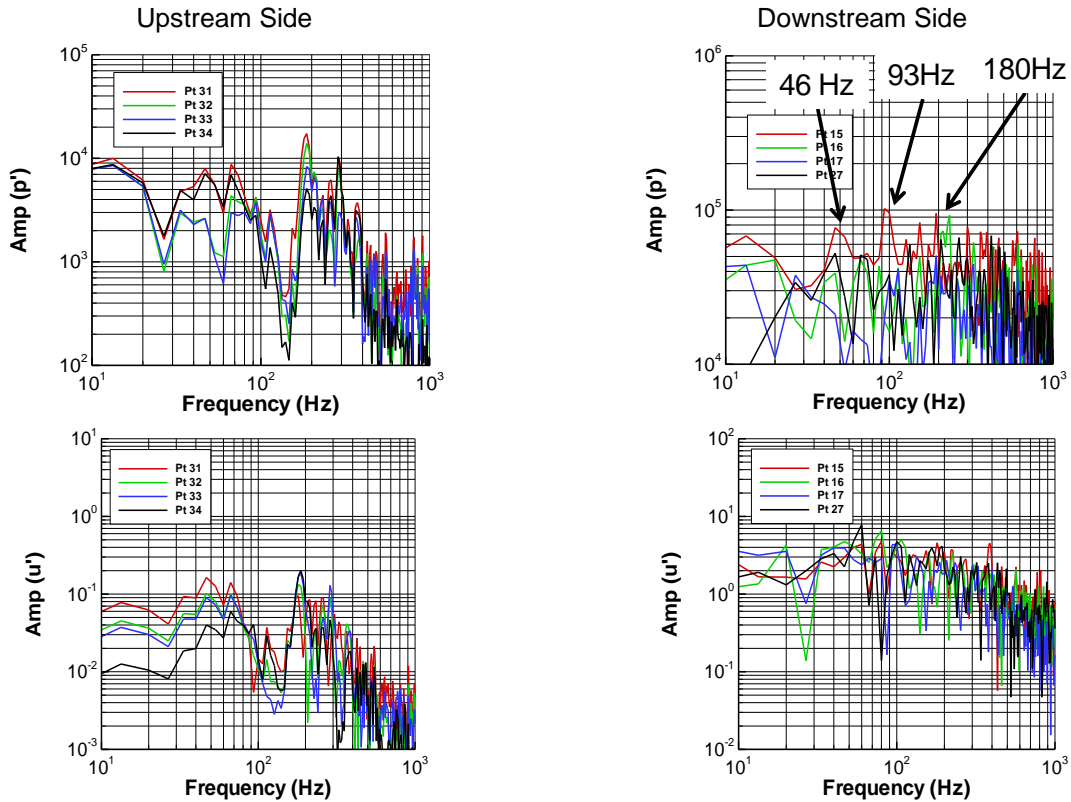

Figure 15. Pressure and velocity spectra at the upstream and downstream probe points.

The amplitudes of the pressure and velocity at the low frequency (46 Hz) and high frequency (180 Hz) for both points are extracted from their respective spectra and used to determine the coefficients of the transfer matrix given by the system below. As was shown previously in the discussion of the transfer matrix the subscript 2 stands for the fluctuations at the downstream end and the subscript 1 refers to the fluctuations at the upstream end. The amplitudes at the two dominant frequencies from the CFD simulations are used to solve the linear system of equations, thereby obtaining the coefficients of the transfer matrix. Both the pressure and velocity fluctuations downstream of the orifice show relatively greater dependence on the velocity fluctuation upstream of the orifice. This is also seen in the analytically derived expressions for the orifice that were discussed previously.

$$\begin{bmatrix} p_2' \\ u_2' \end{bmatrix} = \begin{bmatrix} T_{11} & T_{12} \\ T_{21} & T_{22} \end{bmatrix} \begin{bmatrix} p_1' \\ u_1' \end{bmatrix} \tag{20}$$

where

$$T = \begin{bmatrix} 3.97 & 2.7e5 \\ 1.6e-4 & 1.9e1 \end{bmatrix} \tag{21}$$

11

SIMULATION OF A TEST LOOP WITH MULTIPLE COMPONENTS

In this task we demonstrate the ability of the instability analysis framework to analyze a scaled down test loop with more than one component. The scaled down facility is shown in Figure 16, and comprises of a duct component, an orifice, a 90° bend, and a conical expansion (diffuser). The pipe system has input pressure and streamwise velocity fluctuation magnitudes $|p_1'| = 200 \, psi$ and $|u_1'| = 5 \, m/s$, respectively. Other parameters are given for the liquid fluid as $\rho_0 = 1000 \, kg/m^3$, $c_0 = 1200 m/s$, mean input pressure $P_0 = 800 \, psi$ and mean input velocity $U_0 = 20 \, m/s$.
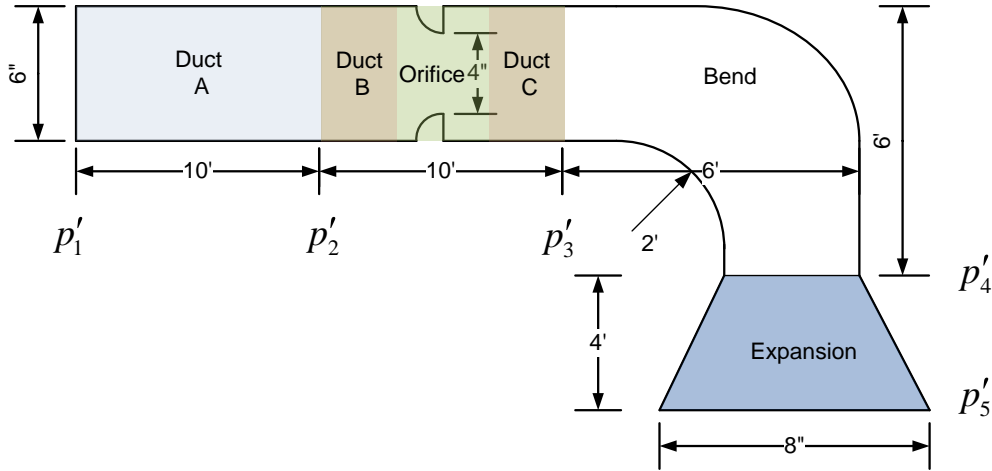
**Figure 16. A schematic of a scaled down system with multiple components (drawing not to scale).**

In order to derive the TM representation of the demo pipe system, it is assumed that the orifice is located in the middle of the orifice pipe section, as shown in Figure 16. Furthermore, the orifice component is assumed to occupy two pipe diameters upstream (i.e., Duct B) and two pipe diameters downstream (Duct C). The length of the downstream Duct C, in particular, depends upon the length of the mixing region. For the bend section, because it is a smooth bend ($r > 3D$), it is thus treated as a duct component as explained earlier. The physical motivation for this comes from the lack of a significant separation bubble size for smooth bends but, again, is expected to be dependent on flow Reynolds number and surface roughness. This model can be fine tuned with the aid of RANS CFD simulations and/or experiments. Consequently, the TM representation for this scaled down system is given by a serial product of the respective transfer matrices of each component

$$\begin{bmatrix} p_5' \\ u_5' \end{bmatrix} = \underbrace{\text{Expansion} \quad \text{Bend} \begin{bmatrix} \text{Duct} \\ \text{C} \end{bmatrix} \text{Orifice} \begin{bmatrix} \text{Duct} \\ \text{B} \end{bmatrix} \begin{bmatrix} \text{Duct} \\ \text{A} \end{bmatrix}}_{\text{Product of transmission matrix of each component}} \begin{bmatrix} p_1' \\ u_1' \end{bmatrix} \quad (22)$$

Figure 17 shows the TM prediction for the amplitude of the perturbation pressure and velocity at the outlet of the duct A $p_2{}', u_2{}'$ and the expansion $p_5{}', u_5{}'$ versus frequency, as indicated in Figure 16. In this case, the pressure p_1' and velocity u_1' perturbations are in phase. The amplitude of the perturbation pressure and velocity are normalized by $|p_1'|$ and $|u_1'|$, respectively. The results indicate that at certain frequencies, the perturbation pressure within the system at a given location can reach a local maximum. In other words, the system (section) is resonant at these frequencies, which could lead to large fluctuating forces on the piping system. For instance, Duct A is resonant at 100 Hz for the given

12

conditions. Figure 18 shows the TM prediction for a similar case when p_1' and u_1' are out of phase by 90°. The change of the excitation condition, which is dependent on components upstream of Duct A, shifts slightly the resonant frequency(ies) of the system (section).

This model has multiple benefits. These results can be used to predict potential frequencies of oscillation or resonance. If the resonant frequencies are near the estimated resonant frequencies of the piping system (obtained from a modal structural analysis), then the geometry of system components can be adjusted to "detune" the respective frequencies away from each other. Furthermore, as additional data (experimental or CFD) are compiled, the TM model can be adjusted to improve its accuracy.
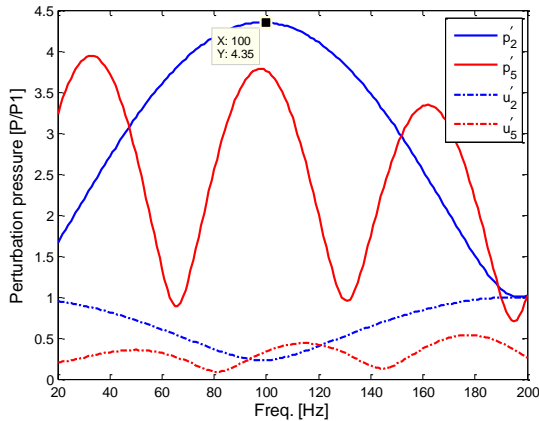
Figure 17. Perturbation pressure and velocity within a demo pipe system with p_1' and u_1' in phase.
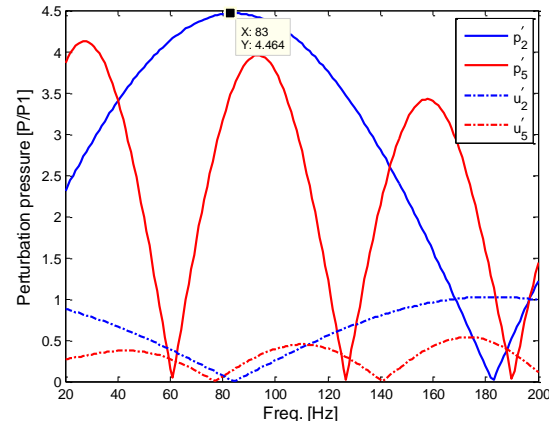
Figure 18. Perturbation pressure and velocity within a demo pipe system with p_1' and u_1' out of phase by 90°.

SUMMARY AND CONCLUSIONS

In summary, the significance of this paper is the development of a multi-level tool that can resolve a governing instability in a liquid rocket propulsion system or test facility, and identify modes that amplify as the instability travels through the various components that comprise the system. The primary source of the unsteadiness is modeled with a high-fidelity hybrid RANS/LES based CFD methodology that has been previously used to study instabilities in feed systems, such as in orifices/ventures and transient valve operation in test facilities. System response to the instability can be predicted through the use of a transfer matrix approach where the individual responses of all the components in the system can be integrated together in real-time to identify potentially harmful resonant modes. The resultant multi-level tool can be used to mitigate these resonant modes by providing design support for (i) alternate system configurations and/or (ii) control mechanisms for suppression of the resonant modes.

The focus of this paper relates to the development of a system level tool based on the Transfer Matrix approach for the evaluation of a propagating instability. The transfer matrix is used to link the pressure and velocity fluctuations at the inlet of a given component with the analogous fluctuations at the exit of the component. The coefficients of the transfer matrix are derived rigorously from one-dimensional wave theory principles based on the dominant flow physics characteristic of the component. Transfer Matrices were derived for components that are commonly seen in rocket engine systems/test stands such as pipe systems that consist of straight ducts and 90° bends, flow control elements, such as orifices, and variable area ducts, such as nozzles and diffusers. One of the major advantages of the transfer matrix approach is that the propagation of a disturbance through a system loop can be analyzed by assembling a simple product of the transfer matrices of the components that comprise the system. An integral part of this paper involved the demonstration of the propagation of an instability through a system that consisted of a straight duct, an orifice, a turning duct and an exit diffuser.

13

Approved for public release; distribution is unlimited.

RELEASED - Printed documents may be obsolete; validate prior to use.

One of the important goals of the program was to utilize high-fidelity CFD to understand the important flow physics responsible for the governing instability and to characterize the important modes associated with hydrodynamic instability. Having characterized the instability with high-fidelity CFD, the next goal was to determine a procedure for utilizing this information with the transfer matrix approach used for propagating the instability through all the components that comprise a propulsion system loop. To this end, three-dimensional simulations with the hybrid RANS-LES model were carried out for an orifice operating with liquid oxygen. Simulations of the orifice show periodic shedding from the lip of the orifice resulting from the onset of the Kelvin Helmholtz instability and the important modes were identified as part of the simulation. Furthermore, information from the CFD simulations was used to construct the coefficients of a transfer matrix. This transfer matrix can be embedded in the system level tool discussed in the paper to investigate dynamic behavior of rocket engine systems and test facilities.

ACKNOWLEDGMENTS

REFERENCES

[1] Ahuja, V., Hosangadi, A., Cavallo, P.A., Ungewitter, R.J., and Shipman, J. **Simulations of Unsteady Valve Systems**, FEDSM2005-77447, 2005 ASME Fluids Engineering Summer Conference, Fifth International Symposium on Pumping Machinery, Houston, TX, June 19-23, 2005.

[2] Cavallo, P.A., Ahuja, V., and Hosangadi, A., **Transient Simulations of Valve Motion in Cryogenic Systems**, Paper No. AIAA-2005-5152, 35th Fluids Dynamic Conference, Toronto, Ontario, CA, Jun. 6-9, 2005.

[3] Ahuja, V., Hosangadi, A., Cavallo, P.A. and Daines, R. **Analyses Of Transient Events In Complex Valve and Feed Systems**, Paper No. AIAA-2005-4549, 41st AIAA/ASME/SAE/ASEE Joint Propulsion Conference & Exhibit, 10 - 13 Jul 2005, Tucson, Arizona.

[4] Arunajatesan, S. and Sinha, N., **Hybrid RANS-LES Modeling for Cavity Aeroacoustics Predictions**, *International Journal of Aeroacoustics*, Vol. 2, No. 1, pp 65-91, 2003.

[5] Ahuja, V., Cavallo, P. A., Shipman, J.D., Lee, C.P. and Hosangadi, A., **Modeling Chatter in a Pressure Regulator Valve With a Multi-Physics Simulation Framework**, 44th AIAA/ASME/SAE/ASEE Joint Propulsion Conference & Exhibit, Hatford, CT, AIAA Paper No. AIAA-2008-4669, 20-23, JUL 2008.

[6] Hosangadi, A. and Ahuja, V., **Numerical Study Of Cavitation In Cryogenic Fluids**, *Journal of Fluids Engineering*, Vol. 127, pp. 267-281, March 2005.

[7] Gallas, Q., Holman, R., Nishida, T., Carroll B, Sheplak, M., and Cattafesta, L., **Lumped Element Modelling of Piezoelectric-Driven Synthetic Jet Actuators**, *AIAA Journal*, Vol. 41, No. 2, pp. 240-247, 2003.

[8] Munjal, M.L., **_Acoustics of ducts and mufflers with application to exhaust and ventilation system design_**, Wiley-Interscience, 1987.

[9] Brennen, C., and Acosta, A.J., **The Dynamic Transfer function for a Cavitating Inducer**, J. of Fluids Engineering, *Transactions of the ASME*, V. 98, pp. 182-192, 1976.

[10] Lampton, M., **_Transmission matrices in electroacoustics_**, Acoustica, 39, 1978.

[11] Stewart, G.W., and Lindsay, R.B., **_Acoustics_**, Printed by Multigraph Dept. State University of Iowa, 1925.

14

[12] Ahuja, V, Arunajatesan, S., Erwin, J., Liu, F., and Cattafesta, L., ***Integrated Component and System Analyses of Instabilities in Test Stands***, Contract No. NNX09CF83P, Final Report No. CRAFTR-01.2010.001 (C384), January 21, 2010.

[13] Weston, D.E., ***The theory of the propagation of plane sound waves in tubes***, Proceedings of the Physical Society Section B, 66(8):695-709, 1953.

[14] Tijdeman, H., ***On the propagation of sound waves in cylindrical tubes***, *Journal of Sound and Vibration*, 39(1):1-33, 1975.

[15] Ahuja, K.K., Munro, S., and Gaeta, R.J., Jr., ***Flow Duct Data for Validation of Acoustic Liner Codes for Impedance Eduction***, NASA/CR-2000-210634.

[16] Miles, J.H., ***Acoustic transmission matrix of a variable area duct or nozzle carrying a compressible subsonic flow***, *Journal of Acoustic Society of America*, 69(6), 1981.

[17] Hofmans, C.C.J., Boot, R.J.J., Durrieu, P.O.J.M., and Auregan, Y., ***Aeroacoustic response of a slit-shaped diaphragm in a pipe at low Helmholtz number, 1: quasi-steady results***, *Journal of Sound and Vibration*, 244(1), 2001.

[18] Dequand, S., Van Lier, L., Hirschberg, A. and Huijnen, J., ***Aeroacoustic response of diffusers and bends: comparison of experiments with quasi-steady incompressible flow models***, *Journal of Fluids and Structures*, 16(7), 2002.

15